Journal of Applied Polymer Science

Fabrication of a novel cellulose acetate imprinted membrane assisted with chitosan-wrapped multi-walled carbon nanotubes for selective separation of salicylic acid from industrial wastewater

Minjia Meng,[1] Zhihui He,[1] Li Yan,[2] Yongsheng Yan,[1] Fengquan Sun,[1] Yan Liu,[2] Shijuan Liu[3]

[1]School of Chemistry and Chemical Engineering, Jiangsu University, Zhenjiang 212013, China
[2]School of Chemistry, Jilin Normal University, Siping 136000, China
[3]Yangzhong Jinxiang Latex Co., Ltd., Yangzhong 212200, China
Correspondence to: Y.S. Yan (mmjybyq@aliyun.com)

ABSTRACT: Highly selective cellulose acetate (CA) blend imprinted membranes for salicylic acid (SA) removal were synthesized by phase inversion technique with chitosan as a functional polymer and chitosan-wrapped multi-walled carbon nanotubes (CHI-wrapped MWCNTs) as the additives. The surface and cross-sectional morphology of membranes were strongly affected by the amount of CHI-wrapped MWCNTs. As compared to M_1-MIM, M_2-MIM, and M_4-MIM, the M_3-MIM with 2.0 wt % CHI-wrapped MWCNTs showed higher membrane flux, faster kinetic, binding capacity and better selectivity for SA. The experimental data of adsorption kinetic were well fitted to the pseudo-second-order kinetic model by multiple regression analysis. The M_3-MIM had the maximum adsorption capacity for SA. The selectivity coefficients of SA to *p*-hydroxybenzoic acid (*p*-HB) and acetylsalicylic acid (ASA) over M_3-MIM were 6.3090 and 6.0019, respectively, showing that M_3-MIM had excellent binding affinity and selectivity for separation of SA from SA-contained aqueous solution. © 2015 Wiley Periodicals, Inc. J. Appl. Polym. Sci. **2015**, *132*, 42654.

KEYWORDS: adsorption; membranes; separation techniques

Received 20 January 2015; accepted 15 June 2015
DOI: 10.1002/app.42654

INTRODUCTION

Salicylic acid (SA) is a prominent pharmaceutical intermediate to produce acetylsalicylic acid (aspirin), sodium salicylate, salicylamide, acethxybenzamide, and phenyl salicylate. The consumption of SA for the production of anti-inflammatory drug aspirin is more than 12,000 tons in the United States and more than 30,000 tons in China each year.[1–3] However, the increasing production of SA causes increasing amount of SA-contained industrial wastewater at the same time. Furthermore, general sewage treatment technologies are less effective for removal and recovery of the valuable SA from SA-contained industrial wastewater, which not only causes resources to be wasted but also surface and ground water and even drinking water to be polluted.[4] In these cases, it is of great significance in developing efficient method for separating and enriching of SA from disposal of the SA-contained industrial wastewater.

Molecular imprinting technology (MIT) is applied worldwide to create selective recognition sites into polymer matrix, obtaining molecularly imprinted polymers (MIPs).[5] MIP technology has made some advances in selectively separating various compounds.[6,7] Recently, molecularly imprinted membrane (MIM) has become one of the great important researches in the MIT field.[8] As compared to conventional size-exclusion membranes, the MIM has additional advantages: high selectivity, integrity and stability. Targeted molecules can be easily separated from wastewater by the permeation process of membrane separation, which is beneficial for the effective recycling of valuable materials.[9] Therefore, it is important to develop a novel MIM with high selectivity and adsorption capacity for effective separation and recovery of SA from SA contained industrial wastewater.

Phase inversion technique is a very promising method to fabricate high selectivity and large-scale MIM due to its controllability and simplicity.[10,11] Cellulose acetate (CA) is an excellent membrane material in the treatment of water and wastewater for its high biocompatibility, good scalability, relatively low cost as well as the ease of application.[12–15] However, the application of pure CA membranes is limited due to their drawbacks such as low porosity, low membrane flux, insufficient hydrophilicity and time-consuming. Researchers found that addition of

Additional Supporting Information may be found in the online version of this article.

additives such as Al_2O_3,[16] polyethylene glycol (PEG),[17] ZnO,[18] and polyvinylpyrrolidone (PVP)[19] in the preparation of CA membrane could effectively improve the properties and structure of CA membranes.

Recently, carbon nanotubes (CNTs) have achieved critically important applications in multidisciplinary area,[20] due to the unique characteristics of CNTs such as high aspect ratios, favorable mechanical properties, high thermal stability and novel hollow-tube structures.[21,22] CNTs were found to a good additive in the fabrication of polymer blend membranes, significantly improving the selectivity, permeability and antifouling performance of membranes.[23,24] However, their poor chemical compatibility and inherent insolubility in typical organic solutions limit their applicability. Modification of CNTs with polymers can solve the problems.[22,25] Chitosan (CHI) is an abundant polysaccharide biopolymer with large number of amino and hydroxyl groups, which has been used in the non-covalent surface modification of CNTs.[26] Many studies have revealed that CHI wrapped CNTs could overcome the drawbacks of CNTs dispersion stability. Trigueiro *et al.*[22] used CHI solutions and cellulose nanocrystal (CNC) suspensions to enhance the stability of MWCNTs in aqueous solution, which were used to prepare multilayered hybrid thin membranes through electrostatic layer-by-layer (LBL) self-assembly. The MWCNTs were well dispersed on each layer of the films. Salam *et al.*[25] prepared CHI-wrapped MWCNTs nanocomposite, and found it effectively removing the target metal ions from aqueous solution. Tang *et al.*[27] reported that wet-grinding assisted ultrasonication (GU) method would be an alternative method for preparing CHI-wrapped MWCNTs nanofluid.

Few studies have previously investigated the effect of addition of CHI-wrapped MWCNTs nanofluid on fabrication of CA imprinted membrane for selectively separating SA from SA-contained wastewater. This work focused on the fabrication and characterization of CA blend imprinted membrane *via* phase inversion technique with CA as the membrane matrix, CHI as the functional polymer and CHI-wrapped multi-walled carbon nanotubes (CHI-wrapped MWCNTs) as the additives. Performance of CHI-wrapped MWCNTs nanofluid content in the casting solution on the CA membrane was discussed by membrane morphology, thermal stability, membrane flux, adsorption kinetics, isothermal adsorption and selectivity.

EXPERIMENTAL

Materials

CA, salicylic acid (SA), *p*-hydroxybenzoic acid (*p*-HB), acetylsalicylic acid (ASA), acetic acid (HAc) and dimethyl sulfoxide (DMSO) were obtained from Sinopharm Chemical Reagent (Shanghai, China). The CHI, with a deacetylation degree of 85% was also purchased from Sinopharm Chemical Reagent (Shanghai, China). MWCNTs (purity > 95%, diameter 5–10 nm, length 10–30 μm) were obtained from The Chinese Academy of Sciences, Chengdu Organic Chemistry (Chengdu, China). All materials were used as received. Ultrapure water was used for preparing all aqueous solutions and preservation processes.

Preparation of Membranes

Preparation of CHI-Wrapped MWCNTs Nanofluids. The CHI-wrapped MWCNTs nanofluid was obtained as follows: an amount of 1.0 g of CHI was dissolved in 50 mL of deionized water in the presence of 2.0 vol % of HAc. The mixture was ultrasonicated using tip ultrasound equipment for 30 min and then kept stirring for 24 h at 25°C to obtain the homogeneous solution. Then, 0.25 g of MWCNTs were added to the mixture and stirred for 24 h at 90°C to obtain the homogeneous black nanofluid of MWCNTs wrapped with CHI, finally ultrasoniated for 30 min to increase the homogeneity.

Preparation of CA Blend Imprinted Membrane. First, desired amount of CA was dissolved in DMSO with a constant magnetic stirring for 4.0 h at 40°C to form homogeneous casting solution. Then the pure CA membrane was obtained by the immersion precipitation phase inversion method. After degassing for 24 h, the casting solution was cast on a polished glass substrate at 25°C. After 30 s the cast film was quickly immersed in the non-solvent (water). Finally, the completely formed membrane sheet was subsequently peeled-off and washed using deionized water to remove the residual solvent completely. The pure CA membrane was preserved in deionized water and was designated as M_0.

The whole preparation process of CA blend imprinted membrane is shown in Figure 1. Appropriate amount of black nanofluid of CHI-wrapped MWCNTs were dispersed into DMSO to fabricate CA blend imprinted membrane. Then membrane matrix CA, functional polymer CHI and template SA were added sequentially into the above solvent solution. Then, the resulting solution was stirred for 12 h and ultrasonicated for 1.0 h to break the possible aggregated MWCNTs. Then the casting solution was cast on a polished glass substrate and the CA blend imprinted membrane was prepared using the above phase inversion method. The amount of CHI-wrapped MWCNTs nanofluids with respect to total polymer was varied as 1.0, 1.5, 2.0, and 2.5 wt %, thus the obtained CA blend imprinted membranes were designated as M_1-MIM, M_2-MIM, M_3-MIM, and M_4-MIM, respectively. The CA blend imprinted membranes were prepared according to composition given in Table I.

The MIM was extracted with mixed solvents of methanol and acetic acid (9 : 1, v/v) in a Soxhlet apparatus to remove the template SA. The non-imprinted membrane (NIM) was prepared in the same procedure without SA.

Instrumental Analysis

The pristine MWCNTs and CHI-wrapped MWCNTs were characterized by Fourier transform infrared (FT-IR) spectra and Raman spectra. FT-IR spectra were recorded on a Nicolet Nexus 470 FT-IR apparatus with KBr pellet method (Nicolet, USA). Raman spectra used a WITEC Spectra Pro 2300I spectrometer (England) which configured with an Ar-ion laser and provided a laser beam of 532 nm wavelength.

The surface and cross-sectional micrographs of pure CA and its CHI-wrapped MWCNTs incorporated membranes were obtained by scanning electron microscope (SEM, S-4800). Before photographing, all the membrane samples were

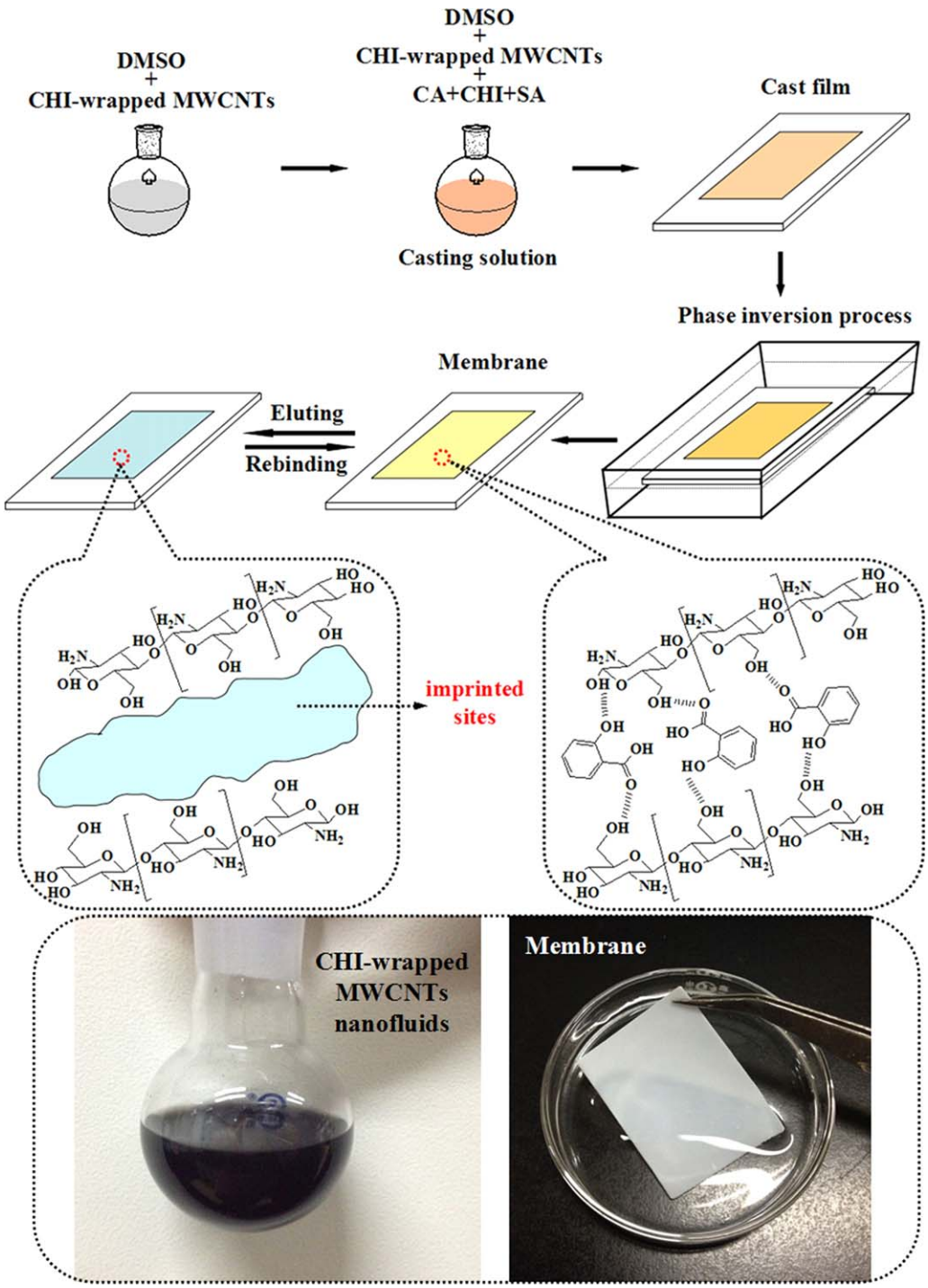

Figure 1. Schematic illustration of preparing blend imprinted membranes by phase inversion technique. [Color figure can be viewed in the online issue, which is available at wileyonlinelibrary.com.]

pretreated with deionized water and vacuum-dried then fractured. After coating with sputtered gold, they were observed with the microscope.

Thermogravimetric analysis (TGA) was performed using a thermogravimetric analyzer (Netzsch STA-449C) at a heating rate of 10°C/min under nitrogen flows. The weight of the samples varied from 1.0 to 2.0 mg.

Membrane Flux Experiments

The membrane flux experiments were conducted using a ultrafiltration cell (UF-8010, Amicon) with 4.9 cm^2 effective membrane area under the operation pressure of 0.15 MPa.[28,29] The aqueous solution containing 50 mg L^{-1} SA was prepared as feed solution. Membranes after compaction were subjected to the testing cell. The feed solution was continuously permeated through the various membranes under certain conditions and

Table I. Membrane Composition for All Prepared CA Blend Membranes

	Composition of casting solution (wt %)				
Membranes	CA	CHI	DMSO	CHI-wrapped MWCNTs nanofluid	SA
M_0-MIM	13	1.0	85.7	0	0.3
M_0-NIM (M_0)	13	1.0	86	0	0
M_1-MIM	13	1.0	84.7	1.0	0.3
M_1-NIM	13	1.0	85	1.0	0
M_2-MIM	13	1.0	84.2	1.5	0.3
M_2-NIM	13	1.0	84.5	1.5	0
M_3-MIM	13	1.0	83.7	2.0	0.3
M_3-NIM	13	1.0	84	2.0	0
M_4-MIM	13	1.0	83.2	2.5	0.3
M_4-NIM	13	1.0	83.5	2.5	0

the membrane flux J (mL cm^{-2} min^{-1}) was calculated by Eq. (1):[30]

$$J=\frac{V}{st} \tag{1}$$

where V (mL) represents volume of permeate solution, t (min) and s (cm^2) represent sampling time and effective area of membrane, respectively.

Batch Mode Adsorption Experiments

To determine the adsorption equilibrium time and the rate-limiting factor of pretreated CA membranes towards the template SA, adsorption kinetics experiments were performed at 25°C. The pretreated membranes were put into 10 mL centrifuge tubes containing 9.0 mL of SA solutions (100 mg L^{-1}). The mixtures were fixed on a constant temperature shaker and shaken for different time periods (0–5 h). After adsorption, the concentrations of SA in the solutions were determined by UV spectrophotometer at a wavelength of 303 nm. The binding amounts (q, mg g^{-1}) were defined in Eq. (2) and the curves of binding amount versus time were obtained.

$$q=\frac{(C_0-C_t)V}{W} \tag{2}$$

where C_0 and C_t (mg L^{-1}) represent the feed concentration at initial time and sampling time t, respectively. V (mL) and W (g) represent the volume of the solution and weight of the prepared membrane, respectively.

SA methanol-water solutions of different concentrations varying from 25 to 300 mg L^{-1} were prepared as the test solution for the batch binding experiment of the MIM and NIM. Batch binding experiments were performed in 10 mL centrifuge tubes containing pretreated membranes and 9.0 mL of test solutions. These centrifuge tubes were placed in 25°C water bath for 3.0 h. Then the residual concentrations of SA in the solutions were analyzed by the UV spectrophotometry. Finally, the equilibrium binding amounts (q_e, mg g^{-1}) were calculated with Eq. (3):

$$q_e=\frac{(C_0-C_e)V}{W} \tag{3}$$

where C_0 and C_e (mg L^{-1}) represent the feed concentration at initial time and saturated binding time, respectively. V (mL) and W (g) represent the volume of the solution and the weight of the prepared membrane, respectively.

Selective Recognition Experiments

The selective properties of membranes were evaluated by performing selective recognition experiments using solutions containing SA and its similar compounds *p*-HB or ASA. A piece of membrane was added into a 10 mL centrifuge tube, each of which contained 9.0 mL the coexisting compound solution with 15 mg L^{-1} of SA and contrast substance (*p*-HB or ASA), respectively. After adsorption, the concentration of each substrate (SA, *p*-HB, ASA) in the solution was determined by UV spectrophotometry and the binding amount of each substrate was calculated by static adsorption Eq. (3).

The separation effect upon selectivity was evaluated using the distribution coefficients (K_d) and selectivity coefficients (α)[31] of SA relative to *p*-HB and ASA which were calculated using the following equations:

$$K_d=\frac{q_e}{C_e} \tag{4}$$

where K_d (mL g^{-1}) represents the distribution coefficient, q_e (mg g^{-1}) and C_e (mg L^{-1}) represent the equilibrium binding amount and the equilibrium concentration of adsorbate, respectively. The selectivity coefficient α was calculated with the following equation:

$$\alpha=\frac{K_{d(i)}}{K_{d(j)}} \tag{5}$$

where $K_{d(i)}$ and $K_{d(j)}$ represent the distribution coefficient of template and the similar compound, respectively.

Membrane Permeation Experiments

To evaluate the permeability performances of MIM and NIM toward competitive substrates SA and *p*-HB, the permeation experiments were performed in H-model tube installation

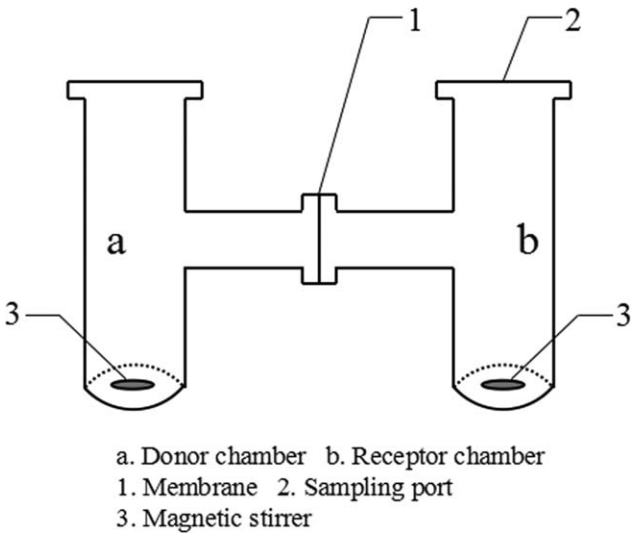

Figure 2. Schematic illustration of H-model tube installation.

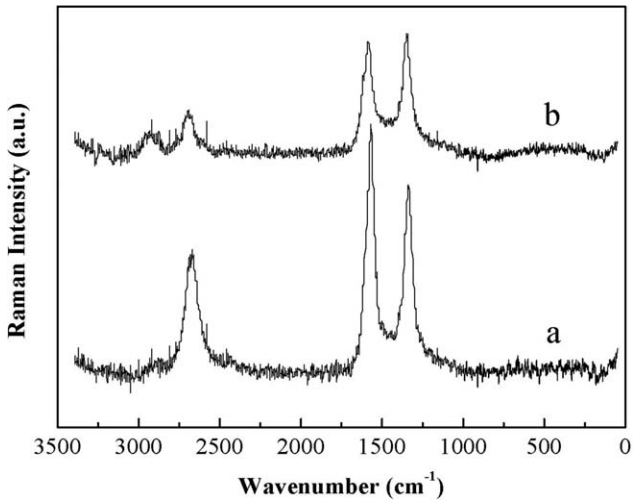

Figure 4. Raman spectra of (a) pristine MWCNTs, (b) CHI-wrapped MWCNTs.

(Figure 2). The volume of each chamber was 150 mL while the effective cross-section area of connection joint of the two test chambers was 1.5 cm^2. The membrane sample was mounted tightly between two chambers.[32] The mixture solution of SA and *p*-HB (95 mL) of 100 mg L^{-1} in methanol/water (3 : 7, v/v) media was placed in the donor chamber, while 95 mL blank methanol/water (3 : 7, v/v) was placed in the receptor chamber. In both chambers, solutions were kept homogeneous by an electromagnetic stirrer at 25°C. The concentration of the substrate that obtained from the receptor solution at sampling time intervals were determined by a UV system. A volume of blank methanol/water (3 : 7, v/v) was added into receptor chamber to maintain a constant volume.

Reusability Experiments

To investigate the regeneration property of the CA blend imprinted membranes the reusability experiments were performed. The cycle experiment of adsorption–desorption was repeated five times by testing the same membranes. The pretreated membranes were tested according to the static adsorption test. Then the concentrations of SA after adsorption were determined by a UV system, the adsorption capacity were obtained by Eq. (3). Afterwards, the membranes were washed with the mixed solvents of methanol and acetic acid (9 : 1, v/v) to remove the template SA for the next adsorption–desorption cycle.

RESULTS AND DISCUSSION

FT-IR and Raman Spectroscopy

FT-IR technique was performed to elucidate the changes in chemical structures. Figure 3 shows the FT-IR spectra of (a) pristine MWCNTs and (b) CHI-wrapped MWCNTs. For pristine MWCNTs, the strong band at 1,575 cm^{-1} indicates the olefinic double bonds. In Figure 3(b) the adsorption bands at 3,370; 1,629; 1,577; and 2,931 cm^{-1} are attributed to —OH group, C═O stretching of residual acetamide groups after the deacetylation, N—H blending modes, and C—H bonding,[33–35] respectively, which indicates CHI wrapped on pristine MWCNTs.

Figure 4 shows the Raman spectra of pristine MWCNTs and the CHI-wrapped MWCNTs. The strong characteristic bands of

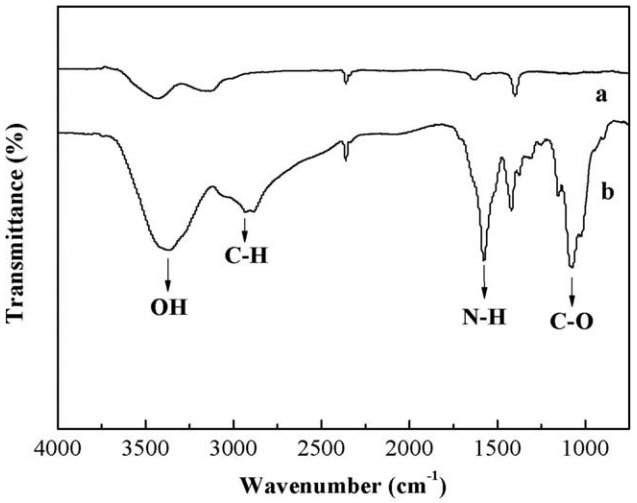

Figure 3. FT-IR spectrum of (a) pristine MWCNTs and (b) CHI-wrapped MWCNTs.

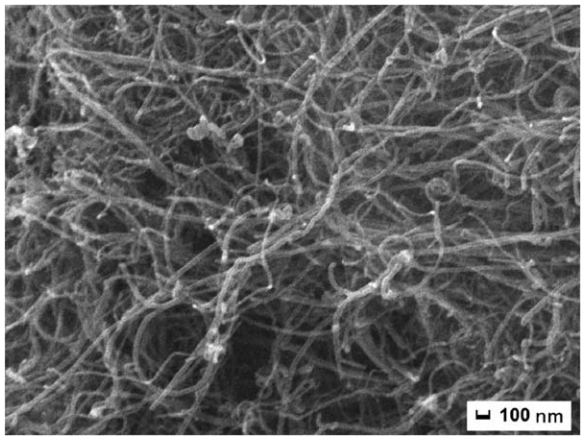

Figure 5. SEM image for pristine MWCNTs.

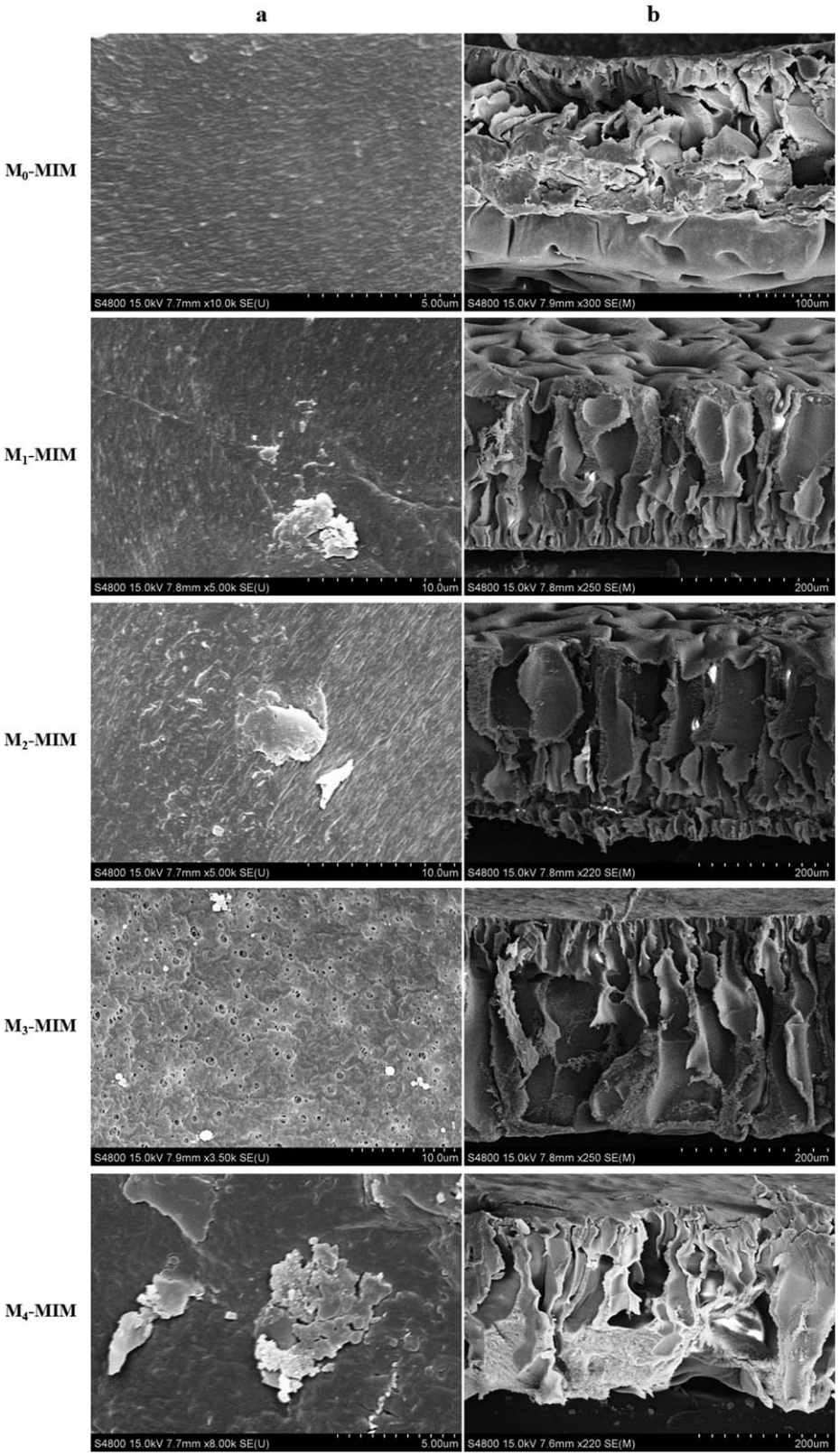

Figure 6. SEM photographs of (a) surface view and (b) cross-sectional view of M_0-MIM, M_1-MIM, M_2-MIM, M_3-MIM and M_4-MIM.

pristine MWCNTs including the adsorptions at 1335 cm^{-1} for the D-band (C—C, the disordered graphite structure) and at 1,575 cm^{-1} for G-band (C═C, sp^2 carbon).[36,37] Compared with pristine MWCNTs, the typical peak at 2,931 cm^{-1} was ascribed to the stretching vibrations of C—H in CHI for CHI-wrapped MWCNTs.

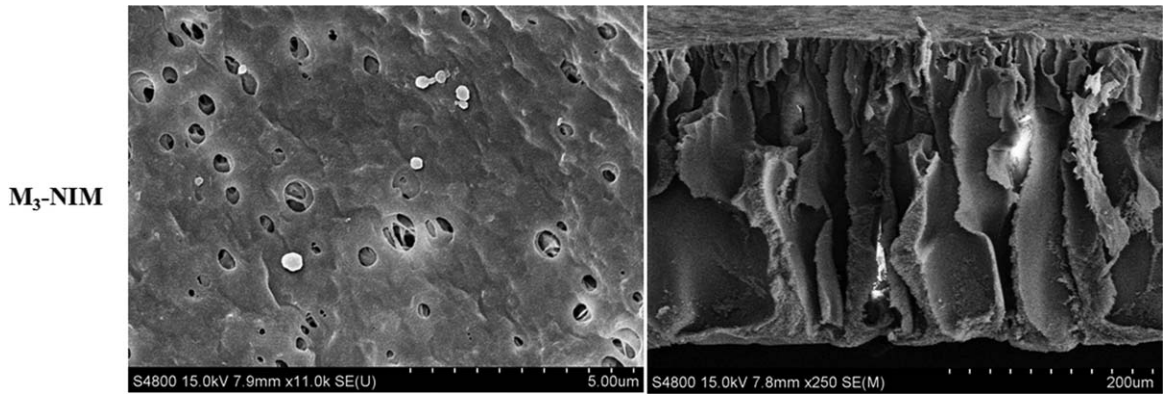

Figure 7. SEM photographs of surface and cross-sectional views of M_3-NIM.

Scanning Electron Microscopy

SEM images were taken to determine the influence of CHI-wrapped MWCNTs content on the membrane morphology.

Figure 5 shows that pristine MWCNTs were tangled together with an average diameter. Figure 6(a,b) present the surface and cross-sectional views of various membranes. As shown in Figure 6(a), with the increase of CHI-wrapped MWCNTs content, the membrane from M_0-MIM to M_4-MIM were changed obviously in surface morphologies. This is due to the more internal nano-channels of MWCNTs and amino and hydroxyl groups of CHI in CHI-wrapped MWCNTs, which resulted in a high diffusional flow between the non-solvent (water) and solvent (DMSO) in the system. Comparing with the morphology of M_0-MIM, M_1-MIM, M_2-MIM, and M_4-MIM, the M_3-MIM containing 2.0 wt % CHI-wrapped MWCNTs exhibited porous surface morphology, which was further confirmed by the EDX results (Supporting Information Figure S1 and Table S1). Therefore, it may have a dual effect on the membrane flux and permeation performance.

Figure 6(b) shows the cross-sectional views of pure CA imprinted membrane (M_0-MIM) and M_1-MIM, M_2-MIM, M_3-MIM, and M_4-MIM. It is clearly shown that the macrovoid and more porous structures are formed with the increase of the content of CHI-wrapped MWCNTs. Further, most CHI-wrapped MWCNTs are well dispersed throughout the CA membranes matrix, suggesting the MIMs possessing good compatibility and incorporation between CHI-wrapped MWCNTs and CA matrix.

Figure 7 shows the surface and cross-sectional views of M_3-NIM. It is also obviously that there are more porous surface and void structure in M_3-NIM. Compared with the photographs of M_3-MIM, there were less difference between the morphology of M_3-NIM and M_3-MIM. The result further proved that the morphologies of membranes were mainly influenced by the content of CHI-wrapped MWCNTs.

Thermal Gravimetric Analysis (TGA)

TGA was carried out to evaluate the degradation behavior and thermal stability of CHI-wrapped MWCNTs incorporated CA imprinted membranes. The resulting TGA plots of MIMs are shown in Figure 8. Additionally, Figure 9 shows the TG-DSC plots of washed M_3-MIM. As shown in Figure 8, it is found that all the membranes exhibited weight loss under nitrogen flow. The first weight loss occurred between room temperature and 60°C, this was mainly due to the loss of an amount of the physically absorbed water molecules. The weight loss is only about 5% for CA imprinted membrane, nevertheless, MIM presented slightly higher loss of about 8%, which could be ascribed

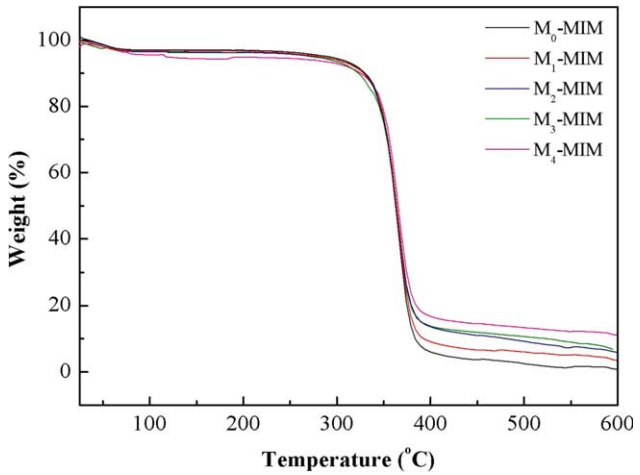

Figure 8. Thermogravimetric analysis for M_0-MIM, M_1-MIM, M_2-MIM, M_3-MIM and M_4-MIM. [Color figure can be viewed in the online issue, which is available at wileyonlinelibrary.com.]

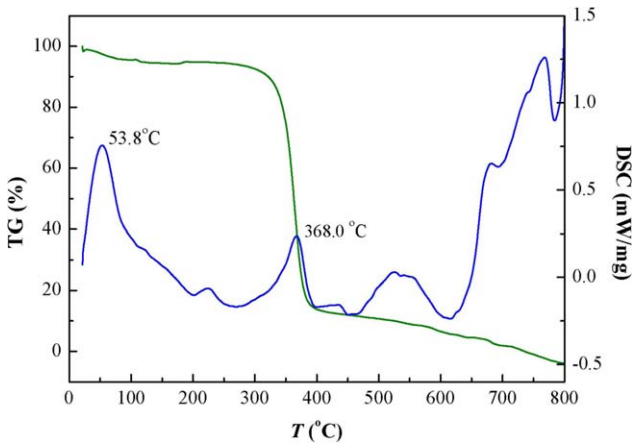

Figure 9. TG-DSC cures of M_3-MIM. [Color figure can be viewed in the online issue, which is available at wileyonlinelibrary.com.]

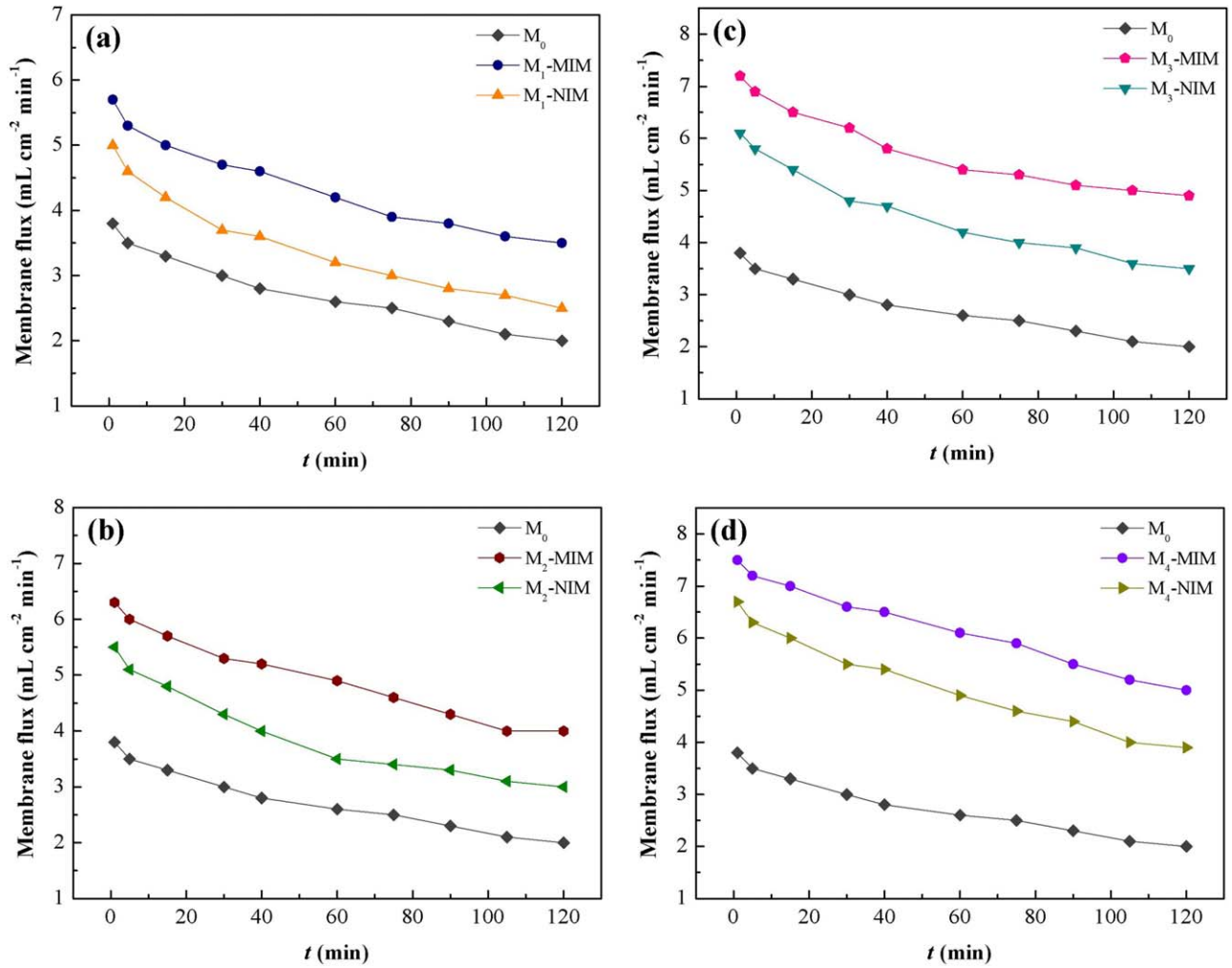

Figure 10. Membrane flux of M_0 and M_1-MIM/NIM (a); M_0 and M_2-MIM/NIM (b); M_0 and M_3-MIM/NIM (c); M_0 and M_4-MIM/NIM (d). [Color figure can be viewed in the online issue, which is available at wileyonlinelibrary.com.]

to the more amino and hydroxyl groups in CHI-wrapped MWCNTs incorporated membranes. This result reveals that membranes incorporated with CHI-wrapped MWCNTs have higher water retention capacity. From Figures 8 and 9, the rapid decomposition of the polymer happened beyond the temperature 335°C, which is corresponding to the degradation of CA and wrapped CHI. Considering the temperature of 80% weight loss as a measuring point, the CHI-wrapped MWCNTs incorporated CA imprinted membranes showed around 20–30°C higher than that of pure CA imprinted membrane. This result suggests that CA blend membranes in the presence of CHI-wrapped MWCNTs exhibited higher thermal decomposition temperature.

Membrane Flux Experiments

Membrane flux is considered to be the key membrane characteristics that determine the membrane performance. After compaction, the membrane flux was measured at the transmembrane pressure of 0.15 MPa and the results were presented in Figure 10.

As shown in Figure 10(a), the M_0 has the lowest membrane flux, which could be attributed to the tight polymer structure and small size pores of pure CA membrane. Compared with the flux of M_0, M_1-MIM, and M_1-NIM produced higher flux values at beginning while declined later, which was possible due to the more pores in M_1-MIM and M_1-NIM consistent with the results observed in the SEM study. Then, the pores will be gradually jammed with the increase of operation time as well as the adsorption of SA. In addition, the M_1-MIM exhibited higher membrane flux compared to M_1-NIM at similar pressure, suggesting M_1-MIM beneficial to the recognition capability and mass transport for SA.

The effect of the addition of different amount of CHI-wrapped MWCNTs in the CA membranes on the flux was investigated detail in Figure 10. As expected, the flux profiles of M_2-MIM (or M_2-NIM), M_3-MIM (or M_3-NIM) and M_4-MIM (or M_4-NIM) all exhibited high membrane flux of MIM [see Figure 10(b–d)]. The total membrane flux was increased remarkably with the increasing amount of CHI-wrapped MWCNTs in the membranes. This is mainly due to the large number of —OH, $—COO^-$ and $—NH_2$ groups in CHI-wrapped MWCNTs, which increased the interaction between water molecules and blend membranes. Furthermore, the incorporation of CHI-wrapped

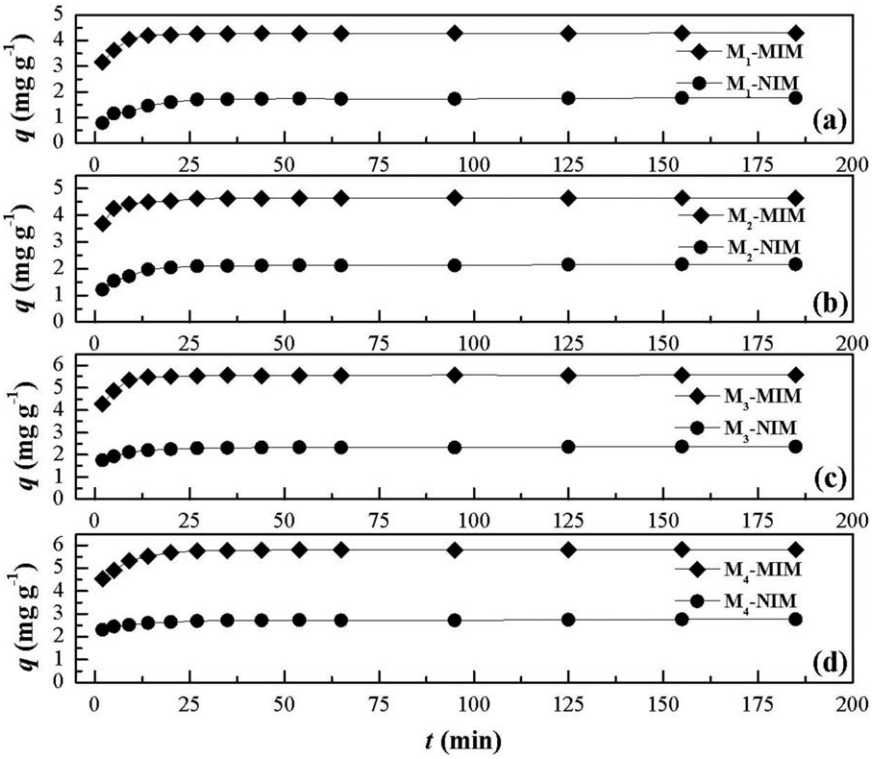

Figure 11. Comparison of the adsorption kinetics of different membranes: (a) M_1-MIM and M_1-NIM, (b) M_2-MIM and M_2-NIM, (c) M_3-MIM and M_3-NIM and (d) M_4-MIM and M_4-NIM.

MWCNTs could create internal nano-channels in the blend membranes due to MWCNTs, and thereby lead to increase the membrane flux. Consequently, the CHI-wrapped MWCNTs could easily enhance the permeate rate and improve the membrane flux of MIM.

Batch Adsorption Kinetics

The adsorption rate is a crucial parameter used to reflect the adsorption process. Figure 11 shows the adsorption kinetic curves of SA on MIM (M_1-MIM, M_2-MIM, M_3-MIM, M_4-MIM) and NIM (M_1-NIM, M_1-NIM, M_1-NIM, M_4-NIM) from methanol aqueous solution containing 100 mg L^{-1} SA at different sampling time. The adsorption equilibrium time of MIM and NIM were 10 and 25 min, respectively. It reveals that the MIM reached the adsorption equilibrium faster than NIM due to the large amount of specific imprinting cavities in MIM. Moreover, the adsorption amounts of SA on MIM increased rapidly in the first few minutes, and then, the adsorption amounts increased slowly and reached equilibrium. It is speculated that a large number of high-affinity binding sites existing in the imprinted membrane. It will be easier for MIM to recognize and bind with the template SA in the initial time. After a while, a gradual decrease of adsorption rate of SA on MIM will be occurred with the increasing diffusion resistance.

In this work, it was found that the adsorption kinetic of M_3-MIM for SA was much higher than that of other corresponding imprinted membranes. The results suggested that M_3-MIM with 2.0 wt % CHI-wrapped MWCNTs was more suitable to improve the adsorption of SA.

For further investigate the underlying mechanism of adsorption processes, the kinetics of SA adsorption on M_3-MIM and M_3-NIM were analyzed by two typical kinetic models: the pseudo-first-order [Eq. (6)] and pseudo-second-order rate equation [Eq. (7)].[38] The pseudo-first-order model can be described in following equation:

$$q_t = q_e - q_e e^{-k_1 t} \tag{6}$$

where q_e and q_t (mg g^{-1}) represent the adsorption capacity at equilibrium and any time t (min), respectively. k_1 (min^{-1}) present the pseudo-first-order rate constant of adsorption.

Table II. Kinetics Constants for the Pseudo-First-Order and Pseudo-Second-Order Equations

	Pseudo-first-order model				Pseudo-second-order model		
Adsorbents	$q_{e,exp}$ (mg g^{-1})	$q_{e,cal}$ (mg g^{-1})	k_1 (min^{-1})	R^2	$q_{e,cal}$ (mg g^{-1})	k_2 (g mg^{-1} min^{-1})	R^2
M_3-MIM	5.5704	5.4985	0.7005	0.8236	5.6250	0.2834	0.9716
M_3-NIM	2.3611	2.2804	0.6411	0.6608	2.3493	0.5329	0.9539

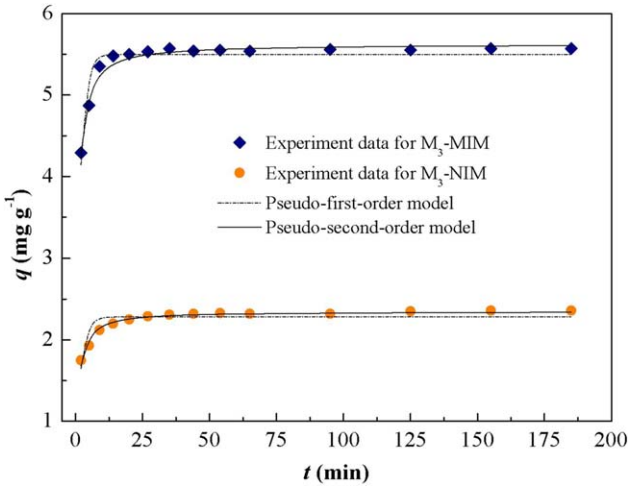

Figure 12. The non-linear regression of kinetic models for M_3-MIM and M_3-NIM. [Color figure can be viewed in the online issue, which is available at wileyonlinelibrary.com.]

The pseudo-second-order model can be expressed as follows:

$$q_t = \frac{k_2 q_e^2 t}{1 + k_2 q_e t} \quad (7)$$

k_2 (g mg^{-1} min^{-1}) present the pseudo-second-order rate constant of adsorption.

The pseudo-first-order kinetic model was used to render the rate of occupation of the imprinting sites in proportion to the number of unoccupied sites. The pseudo-second-order model was perfectly suitable to describe the reaction mechanisms and the adsorption rate due to the sharing and exchange of electrons between the functional polymer and the template.

In this study, the adsorption kinetic constants and nonlinear regression values were listed in Table II, and the nonlinear regression plots of the two models for SA binding were presented in Figure 12. The correlation coefficient (R^2) was used to judge the applicability of the kinetic models. As shown in Table II, the correlation coefficient values (R^2 values above 0.95) of the adsorption process on M_3-MIM or M_3-NIM by pseudo-second-order kinetic model are higher than that by pseudo-first-order model. The pseudo-second-order model exhibited the favorable agreement between the theoretical q_e values ($q_{e,cal}$) and the experimental q_e values ($q_{e,exp}$), while the opposite result was found for the pseudo-first-order model. Therefore, the results suggested that the pseudo-second-order kinetic model was well-described the adsorption behavior of SA.

Adsorption Isotherm

To evaluate the binding performance of the MIM and NIM for SA, the adsorption isotherm experiments were carried out at 25°C, as shown in Figure 13. It can be seen that equilibrium adsorption capacities increased gradually with the increase of the SA initial concentration, and ultimately reached an equilibrium value due to the saturation of static adsorption behavior. Moreover, the MIM exhibited higher adsorption capacity than that of NIM, which was due to a great deal of specific imprinting sites in MIM, thus SA molecules were more easily binding with MIM. In contrast, the NIM showed non-selective adsorption toward SA molecules. It can also be observed that the

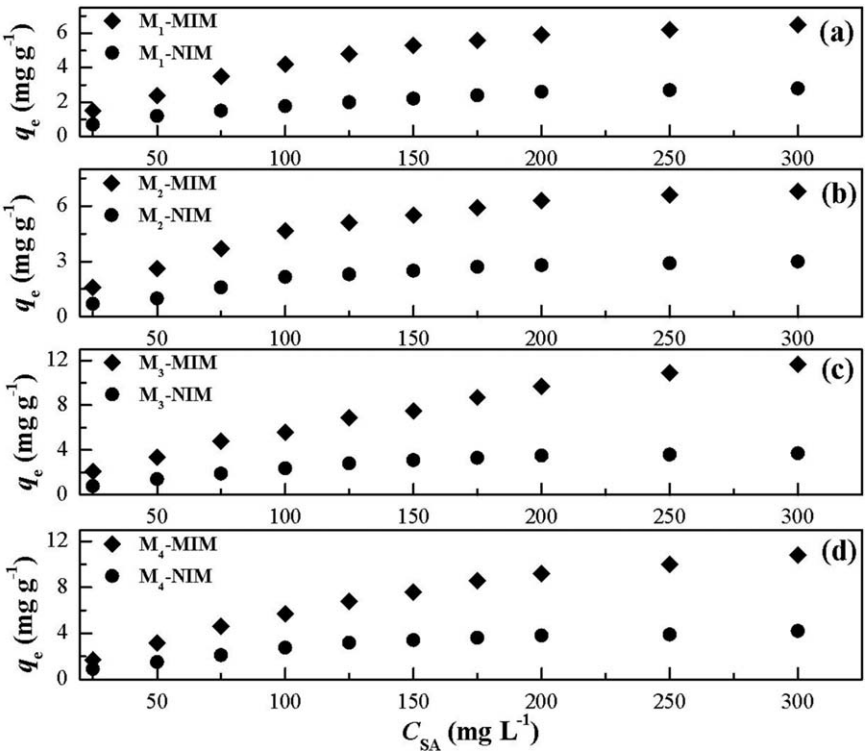

Figure 13. Comparison of the adsorption isotherms of different membranes: (a) M_1-MIM and M_1-NIM, (b) M_2-MIM and M_2-NIM, (c) M_3-MIM and M_3-NIM and (d) M_4-MIM and M_4-NIM.

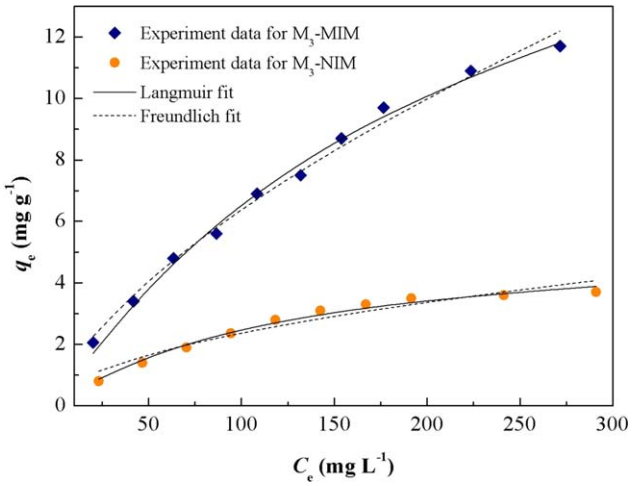

Figure 14. Adsorption isotherms of SA on the M_3-MIM and M_3-NIM with the fitting to the Langmuir model and the Freundlich model. [Color figure can be viewed in the online issue, which is available at wileyonlinelibrary.com.]

adsorption capacity of M_3-MIM toward SA was much higher than that of M_1-MIM, M_2-MIM, and M_4-MIM. It is suggested that the MIM with 2.0 wt % CHI-wrapped MWCNTs was the optimal imprinted membrane in the previous experiment, and this is in accordance with the results observed in the SEM analysis. The morphology and membrane structure were strongly influenced by the content of CHI-wrapped MWCNTs, and the results displayed that 2.0 wt % CHI-wrapped MWCNTs was suitable to generate specific binding in imprinting sites.

In this study, the equilibrium data for SA onto M_3-MIM and M_3-NIM were fitted by two classical isotherm models, i.e., The Langmuir model [Eq. (8)][39] and Freundlich model [Eq. (9)].[40]

$$q_e = \frac{q_m K_L C_e}{1 + K_L C_e} \tag{8}$$

$$q_e = K_F C_e^{1/n} \tag{9}$$

where C_e (mg L^{-1}) represents the equilibrium concentration of SA. q_e (mg g^{-1}) and q_m (mg g^{-1}) represent the equilibrium amount and the maximum adsorption capacity of SA, respectively. K_L is the Langmuir constant related to the affinity of the adsorption sites. K_F and $1/n$ are Freundlich constants related to the capacity and intensity of the adsorption, respectively.

Table III. The Adsorption Isotherm Constants for M_3-MIM and M_3-NIM at 25°C

Adsorption isotherm models	Parameters	M_3-MIM	M_3-NIM
Langmuir model	R^2	0.9938	0.9839
	K_L (L mg^{-1})	0.0042	0.0081
	$q_{m,cal}$ (mg g^{-1})	22.2597	5.5434
Freundlich model	R^2	0.9909	0.9347
	K_F (mg g^{-1})	0.3240	0.2289
	n	1.5448	1.9702

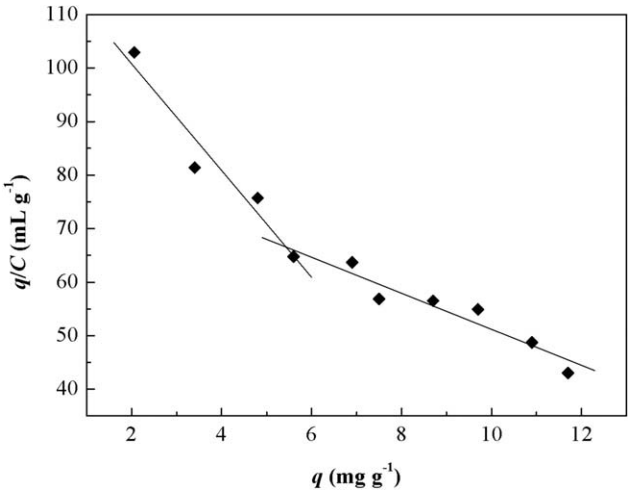

Figure 15. Scatchard curve for M_3-MIM.

A comparison of the isotherm models for SA adsorption onto M_3-MIM and M_3-NIM with nonlinear regression are shown in Figure 14 and the adsorption isotherm constants are given in Table III. The correlation coefficient (R^2) was used to judge the applicability of the isotherm models. As shown in Table III, the experimental data were well fitted by the two models (Langmuir and Freundlich models) with R^2 values: 0.9938, 0.9839; 0.9909, 0.9347 for M_3-MIM and M_3-NIM, respectively. Apparently, the correlation coefficient is higher with the Langmuir model than that with the Freundlich model, which indicated that the Langmuir model provided better fitting for M_3-MIM and M_3-NIM, respectively. The calculated maximum adsorption capacities of M_3-MIM and M_3-NIM were 22.2597 mg g^{-1} and 5.5434 mg g^{-1}, respectively.

In addition, the binding affinity and the theoretical binding site number for template of M_3-MIM was further evaluated by Scatchard analysis.[41] The equation is as follows:

$$\frac{q}{C} = \frac{(q_{max} - q)}{K_d} \tag{10}$$

where q (mg g^{-1}) represents the equilibrium adsorption capacity of SA on M_3-MIM, q_{max} (mg g^{-1}) represents the maximal adsorption capacity of M_3-MIM for SA, C (mg mL^{-1}) represents the SA concentration in the test solution, and K_d (mg mL^{-1}) represents the dissociation equilibrium constant.

Figure 15 shows the Scatchard plot of the adsorption of M_3-MIM for SA. Linear regression analysis yielded two distinct linear sections within the plot of q/C on the vertical axis and C on the horizontal axis. This result indicated that there were two types of binding sites in respect to the affinity for SA of the M_3-MIM. As shown in Table IV, the two sets of binding parameters ($K_{d1} = 0.10$ mg mL^{-1}, $q_{max1} = 12.11$ mg g^{-1} and $K_{d2} = 0.30$ mg mL^{-1}, $q_{max2} = 25.24$ mg g^{-1}) were determined by the slopes and intercepts with the horizontal axis, which was corresponding to the high-affinity and low-affinity binding sites.

Selectivity Binding

The selective adsorption ability of prepared membranes were evaluated toward competitive substrates SA, *p*-HB, and ASA.

Table IV. Results of the Scatchard Analysis

Binding site	Linear equation	K_d (mg mL^{-1})	q_{max} (mg g^{-1})
Higher affinity sites	$q/C = 120.73\text{-}9.97q$ ($R^2 = 0.9121$)	0.10	12.11
Lower affinity sites	$q/C = 84.82\text{-}3.36q$ ($R^2 = 0.9064$)	0.30	25.24

Table V. Parameters of Batch Adsorption Selectivity of Prepared Membranes

	SA			*p*-HB	
Membrane	q_{SA} (mg g^{-1})	K_{dSA} (L g^{-1})	α	$q_{p\text{-HB}}$ (mg g^{-1})	$K_{d(p\text{-HB})}$ (L g^{-1})
M_0	0.2697	0.01798	1.0429	0.2586	0.01724
M_1-MIM	0.9841	0.06560	3.2784	0.3002	0.02001
M_2-MIM	1.1750	0.07833	5.4509	0.2155	0.01437
M_3-MIM	1.4205	0.09470	6.3090	0.2252	0.01501
M_3-NIM	0.7250	0.04833	1.4397	0.5035	0.03357
M_4-MIM	1.3703	0.09135	4.6136	0.2970	0.01980

	SA			ASA	
Membrane	q_{SA} (mg g^{-1})	K_{dSA} (L g^{-1})	α	$q_{p\text{-HB}}$ (mg g^{-1})	$K_{d(ASA)}$ (L g^{-1})
M_0	0.2583	0.01722	1.0023	0.2577	0.01718
M_1-MIM	0.9792	0.06528	3.3684	0.2907	0.01938
M_2-MIM	1.1603	0.07735	5.2619	0.2205	0.01470
M_3-MIM	1.3901	0.09267	6.0019	0.2316	0.01544
M_3-NIM	0.6920	0.04613	1.3832	0.5002	0.03335
M_4-MIM	1.3563	0.09042	4.4740	0.3032	0.02021

The selective binding experiments for the similar compounds on different membranes were all performed under same experimental conditions.

The results of distribution coefficient (K_d) and selectivity coefficient of the sorbent (α) are summarized in Table V. As shown in Table V, the α values of M_0 for SA relative to *p*-HB and ASA were 1.0429 and 1.0023, respectively, indicating that M_0 is almost non-selectivity to SA. Table V also presented that the α values of M_3-MIM for SA relative to *p*-HB and ASA were higher (6.3090 and 6.0019, respectively), and the corresponding α of M_3-NIM were much lower (1.4397 and 1.3832, respectively). Obviously, the above fact fully displayed that MIM had stronger

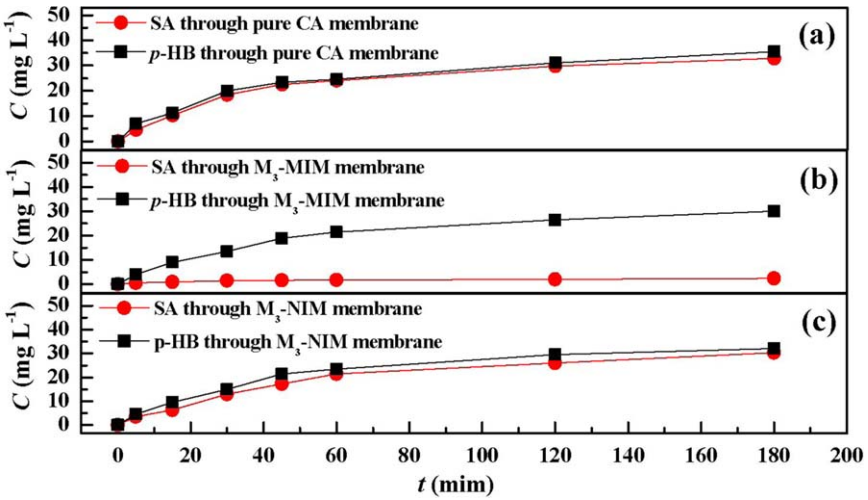

Figure 16. Time-permeation curves of SA and *p*-HB through the various membranes (Feed concentration = 100 mg L^{-1}). [Color figure can be viewed in the online issue, which is available at wileyonlinelibrary.com.]

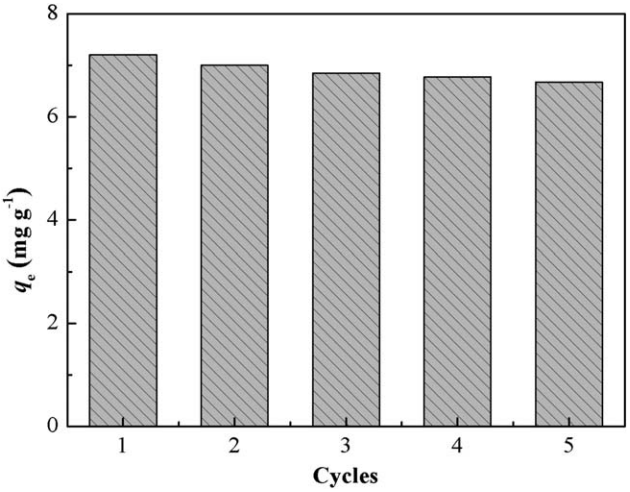

Figure 17. Adsorption-desorption cycles for M_3-MIM.

selective recognition ability than NIM, whereas the separation factor for *p*-HB was higher than that for ASA.

Furthermore, the separation effect of MIM with various concentrations of CHI-wrapped MWCNTs were evaluated and the α values of M_1, M_2, M_3, and M_4-MIM for SA in relation to *p*-HB were 3.2784, 5.4509, 6.3090, and 4.6136, respectively, showing well imprinting effect. It revealed that the CHI-wrapped MWCNTs may be beneficial to improve the effective adsorption sites in the MIM. Clearly, the α value of M_3-MIM was highest among the prepared imprinted membranes, while the α value of M_4-MIM was lower than that of M_3-MIM. It can be obviously seen that the MIM with large amount of CHI-wrapped MWCNTs may not obtain a high selective recognition ability for SA. Excessive CHI-wrapped MWCNTs in M_4-MIM may lead to limit the imprinting effect for SA with the increase of non-specific adsorption. Consequently, the above results suggested that M_3-MIM can be selected as the optimal CA blend imprinted membrane in selective binding experiments.

Membrane Permeation Studies

The permeation concentrations of SA and *p*-HB through pure CA membrane, M_3-MIM and M_3-NIM depending on time were shown in Figure 16. Figure 16(a) shows the time-dependent permeation curves on the pure CA membrane, the concentration of SA and *p*-HB in the receptor chamber were nearly the same, indicating that the pure CA membrane without specific imprinting sites did not have a special selectivity to SA. However, as shown in Figure 16(b), the concentration of *p*-HB was much higher than that of SA for the M_3-MIM, which caused the blocking phenomenon in permeation of SA through the imprinted membrane. The acquirement of this result depends on the specific molecular channel of M_3-MIM to SA and the strong binding interaction between the imprinting sites and SA in the permeation experiments. It was reasonable to assume that templates SA were transported from one specific imprinting site to another until they entered into the receptor chamber, which was accordance with the transport-selectivity diffusion mechanism. It suggested that M_3-MIM could be used to continuously separate templates rather than only absorb specific molecules. Meanwhile, the imprinting sites enable the template analog *p*-HB to permeate through membrane in a continuous way. Figure 16(c) shows the time-permeation plots of SA and *p*-HB on M_3-NIM. It revealed that the diffusion rate of *p*-HB through the NIMs was nearly equal to that of SA. The results showed that non-imprinted membrane M_3-NIM scarcely have the recognition ability to SA and *p*-HB. In addition, it can be also found that the diffusion rate of SA and *p*-HB on M_3-NIM was lower than that of pure CA membrane. It could be explained that M_3-NIM accomplished the diffusion of molecules with abundant non-specific binding sites, which causing a decrease of the diffusion rate of SA and *p*-HB.

Regeneration

To evaluate the stability and regeneration of the M_3-MIM, the regeneration experiment was performed at the SA concentration of 100 mg L^{-1}. After adsorption of SA onto M_3-MIM, the SA-adsorbed M_3-MIM was regenerated using the methanol/acetic acid (9 : 1, v/v) mixed solvent and deionized water. The adsorption capacity of the M_3-MIM adsorbent for SA with five consecutive adsorption-regeneration cycles was shown in Figure 17. It was clearly seen that the adsorption capacity of SA on M_3-MIM decreased gradually for the first three times, and then the adsorption capacity maintained their recovery rate at almost constant value of 92.61%. It is reasonable to assume that the M_3-MIM could be reused at least five times without significant decrease in their adsorption capacities.

CONCLUSIONS

In this work, a series of CA blend imprinted membranes assisted with CHI-wrapped MWCNTs for SA were synthesized by phase inversion imprinting technique. The properties, membrane flux, kinetics, selectivity and regeneration were studied in detail. Morphological analysis and membrane flux showed that the porous structure and hydrophilicity can be improved significantly by increasing the CHI-wrapped MWCNTs concentration. The adsorption kinetic analysis indicated that the CHI-wrapped MWCNTs were beneficial to promote the effective imprinting sites in MIM. The M_3-MIM with 2.0 wt % CHI-wrapped MWCNTs was found to be the optimal imprinted membrane and showed high kinetic equilibrium adsorption capacity for the binding of SA. The pseudo-second-order kinetic model was able to predict the adsorption behavior of SA on M_3-MIM. Moreover, adsorption isotherm studies showed that the M_3-MIM had high binding capacity for SA. The selectivity binding results revealed that the M_3-MIM had prominent selective recognition ability for SA in respect to the competitive analogues. Further studies will be performed to extend this research to separate SA from complex matrix.

ACKNOWLEDGMENTS

This work was financially supported by the National Natural Science Foundation of China (Nos. 21207051, 21406085), Ph.D. Programs Foundation of Ministry of Education of China (No. 20123227120015), Programs of Senior Talent Foundation of Jiangsu University (No. 15JDG024) and Natural Science Foundation of Jiangsu Province (BK20140580), and Special Financial

Grant from the China Postdoctoral Science Foundation (2014T70488).

REFERENCES

1. An, F. Q.; Du, R. K.; Wang, X. H.; Wan, M.; Dai, X.; Gao, J. F. *J. Hazard. Mater.* **2012**, *201*, 74.
2. Spitz, G. A.; Furtado, C. M.; Sola-Penna, M.; Zancan, P. *Biochem. Pharmacol.* **2009**, *77*, 46.
3. Hussain, M.; Javeed, A.; Ashraf, M.; Zhao, Y.; Mukhtar, M. M.; Ur Rehman, M. *Int. Immunopharmacol.* **2012**, *12*, 10.
4. Meng, M. J.; Feng, Y. H.; Zhang, M.; Ji, Y. J.; Dai, J. D.; Liu, Y.; Yu, P.; Yan, Y. S. *Chem. Eng. J.* **2013**, *231*, 132.
5. Blanco, S. G. D.; Donato, L.; Drioli, E. *Sep. Purif. Technol.* **2012**, *87*, 40.
6. Wang, J. Y.; Xu, Z. L.; Wu, P.; Yin, S. J. *J. Membr. Sci.* **2009**, *331*, 84.
7. Huang, J. X.; Hu, Y. F.; Hu, Y. L.; Li, G. K. *Talanta* **2013**, *107*, 49.
8. Zhang, Y. Q.; Shan, X.; Gao, X. Q. *Sep. Purif. Technol.* **2011**, *76*, 337.
9. Meng, M. J.; Feng, Y. H.; Zhang, M.; Liu, Y.; Ji, Y. J.; Wang, J.; Wu, Y. L.; Yan, Y. S. *Chem. Eng. J.* **2013**, *225*, 331.
10. Donato, L.; Greco, M. C.; Drioli, E. *Desalination Water Treat.* **2011**, *30*, 171.
11. Donato, L.; Tasselli, F.; De Luca, G.; Garcia Del Blanco, S.; Drioli, E. *Sep. Purif. Technol.* **2013**, *116*, 184.
12. Ghaemi, N.; Madaeni, S. S.; Alizadeh, A.; Daraei, P.; Vatanpour, V.; Falsafi, M. *Desalination* **2012**, *290*, 99.
13. Idris, A.; Yet, L. K. *J. Membr. Sci.* **2006**, *280*, 920.
14. Ghaemi, N.; Madaeni, S. S.; Alizadeh, A.; Daraei, P.; Vatanpour, V.; Falsafi, M. *Desalination* **2012**, *290*, 99.
15. Alia, M.; Zafar, M.; Jamil, T.; Butt, M. T. Z. *Desalination* **2011**, *270*, 98.
16. Wang, Y.; Yang, L.; Luo, G.; Dai, Y. *Chem. Eng. J.* **2009**, *146*, 6.
17. Zafara, M.; Ali, M.; Khan, S. M.; Jamil, T.; Butt, M. T. Z. *Desalination* **2012**, *285*, 359.
18. Alia, M.; Zafar, M.; Jamil, T.; Butt, M. T. Z. *Desalination* **2011**, *270*, 98.
19. Saljoughi, E.; Mohammadi, T. *Desalination* **2009**, *249*, 850.
20. Shao, D. D.; Hu, J.; Jiang, Z. Q.; Wang, X. K. *Chemosphere* **2011**, *82*, 751.
21. Phuoc, T. X.; Massoudi, M.; Chen, R. H. *Int. J. Therm. Sci.* **2011**, *50*, 12.
22. Trigueiro, J. P. C.; Silva, G. G.; Pereira, F. V.; Lavall, R. L. *J. Colloid Interface Sci.* **2014**, *432*, 214.
23. Vatanpour, V.; Madaeni, S. S.; Moradian, R.; Zinadini, S.; Astinchap, B. *J. Membr. Sci.* **2011**, *375*, 284.
24. Daraei, P.; Madaeni, S. S.; Ghaemi, N.; Khadivi, M. A.; Astinchap, B.; Moradian, R. *J. Membr. Sci.* **2013**, *444*, 184.
25. Salam, M. A.; Makki, M. S. I.; Abdelaal, M. Y. A. *J. Alloys Compd.* **2011**, *509*, 2582.
26. Brito, J. B.; Gomes, D. J. C.; Justina, V. D.; Lima, A. M. F.; Olivati, C. A.; Silva, J. R.; de Souza, N. C. *J. Colloid Interface Sci.* **2012**, *367*, 467.
27. Tang, C. Y.; Zhou, T. N.; Yang, J. H.; Zhang, Q.; Chen, F.; Fu, Q.; Yang, L. *Colloids Surf. B: Biointerfaces* **2011**, *86*, 189.
28. An, Q. F.; Ji, Y. L.; Hung, W. S.; Lee, K. R.; Gao, C. J. *Macromolecules* **2013**, *46*, 2228.
29. Shao, L. L.; An, Q. F.; Ji, Y. L.; Zhao, Q.; Wang, X. S.; Zhu, B. K.; Gao, C. J. *Desalination* **2014**, *338*, 74.
30. Chen, F. S.; Sun, Z. H. *Carbohydr. Polym.* **2013**, *95*, 85.
31. Meng, M. J.; Bao, L. L.; He, M. Q.; Sun, K. Y.; Li, W. B.; Zhao, D. X.; Feng, Y. H.; Yan, Y. S. *J. Appl. Polym. Sci.* **2014**, *40118*, 1.
32. Wu, Y. L.; Yan, Y. S.; Pan, J. M.; Dai, X. H.; Shi, W. D.; Meng, M. *J. Chin. Chem. Lett.* **2014**, *25*, 273.
33. Tang, C. Y.; Chen, N. X.; Zhang, Q.; Wang, K.; Fu, Q.; Zhang, X. Y. *Polym. Degrad. Stab.* **2009**, *94*, 124.
34. Salam, M. A.; Makki, M. S. I.; Abdelaal, M. Y. A. *J. Alloys Compd.* **2011**, *509*, 2582.
35. Tang, C. Y.; Zhou, T. N.; Yang, J. H.; Zhang, Q.; Chen, F.; Fu, Q.; Yang, L. *Colloids Surf. B: Biointerfaces* **2011**, *86*, 189.
36. Zhou, Y.; Yang, H.; Chen, H. Y. *Talanta* **2008**, *76*, 419.
37. Tang, C. Y.; Zhou, T. N.; Yang, J. H.; Zhang, Q.; Chen, F.; Fu, Q.; Yang, L. *Colloids Surf. B: Biointerfaces* **2011**, *86*, 189.
38. Wu, Y. L.; Meng, M. J.; Liu, X. L.; Li, C. X.; Zhang, M.; Ji, Y. J.; Sun, F. Q.; He, Z. H.; Yan, Y. S. *Sep. Purif. Technol.* **2014**, *131*, 117.
39. Xue, Y. J.; Hou, H. B.; Zhu, S. J. *Chem. Eng. J.* **2009**, *147*, 272.
40. Yi, X. S.; Shi, W. X.; Yu, S. L.; Wang, Y.; Sun, N.; Jin, L. M.; Wang, S. *J. Hazard. Mater.* **2011**, *189*, 95.
41. Zhang, Y. Q.; Shan, X.; Gao, X. Q. *Sep. Purif. Technol.* **2011**, *76*, 337.